ARCHIVES OF ELECTRICAL ENGINEERING VOL. 66(1), pp. 121-139 (2017)

DOI 10.1515/aee-2017-0009

Comparison of higher harmonic contents in salient pole synchronous generator with different rotor construction

KRZYSZTOF LUDWINEK, ROMAN NADOLSKI, JAN STASZAK

Kielce University of Technology, Department of Automatic Control and Computer Science
Tysiąclecia P. P. 7, 25-314 Kielce, Poland
tel. +48 41 342 46 82
e-mail: {k.ludwinek / r.nadolski / j.staszak}@tu.kielce.pl

(Received: 05.02.2016, revised: 13.09.2016)

Abstract: The paper presents a comparison of higher harmonics in induced phase voltages of a stator winding in the no-load state of a three-phase 5.5 kVA salient pole synchronous generator. The comparison is carried out for the synchronous generator with different salient pole rotor constructions: a non-skewed solid rotor, a non-skewed solid rotor with radial incisions, and a laminated electrotechnical steel rotor with skewed slots and damping bars. The calculations of higher harmonics are based on the magnetic field distributions in the air gap, which are carried out in a 2D model in a FEMM program and on the induced voltage waveforms in the stator windings registered during experimental investigations of the 5.5 kVA salient pole synchronous generator in the no-load state.

Key words: salient pole synchronous generator, higher harmonics, solid rotor, rotor with radial incisions, laminated rotor

1. Introduction

The distribution of the magnetic flux density in the air gap of a salient pole synchronous generator has an influence on the occurrence of higher harmonics in voltage induced in the stator windings [1-8]. The shape of the stator and rotor magnetic surfaces has an influence on the distribution of the magnetic flux density along the air gap circumference, and the magnetic flux density:

– decreases at the stator and rotor slot opening,

– increases if the length of the air gap decreases.

Knowledge about the effective air gap length allows, for example, an analytically more precise specification of: self- and mutual inductances, the distribution of flux density in the air gap, voltages induced in the stator windings etc. [9-14]. The effective air gap length is calculated from the initial length of the air gap by taking into account the total Carter Factor, which is the sum of two factors [4, 14, 15]. The first factor is calculated by assuming a smooth rotor

surface and taking into account stator slots. The second factor is calculated by assuming a smooth stator surface and with rotor slots. In electrical machines the problem of variations in the distribution of the magnetic flux density due to stator and rotor slot openings was first solved by F.W. Carter in 1901 [16]. Generally, the variations in the distribution of magnetic flux density are taken into account in increases of the initial length of the air gap by means of the Carter factor [4, 14-16]. Variations in the distribution of the magnetic flux density in a one sided uniform air gap (including the slots on the stator or on the rotor side) can be determined:

– by the quotient of minimum to maximum magnetic flux density [14, 15]

$$\frac{B_{\min}}{B_{\max}} = \frac{2u}{1+u^2}, \tag{1}$$

– in relation to the quotient of average to maximum magnetic flux density [4]

$$\frac{B_0}{B_{\max}} = \frac{(u-1)^2}{2(1+u^2)}, \tag{2}$$

where: $B_{\min}$ is the minimum magnetic flux density, $B_{\max}$ is the maximum magnetic flux density, u is the coefficient

$$u = b_s / 2\delta_0 + \sqrt{1+(b_s / 2\delta_0)^2},$$

δ_0 is the initial length of the air gap, b_s is the length of the stator slot opening, B_0 is the average magnetic flux density,

As shown in [4] when assuming no eddy currents and the same length of the air gap, if the relation between the length of the stator slot opening and the stator tooth pitch is $b_s/\tau_s < 0.625$, then an analytical expression of the flux density variations in an air gap can be described as:

– if $0 < \alpha < 0.8\alpha$

$$B(\alpha) = \left(1-\beta-\beta\cos\frac{\pi}{0.8\alpha_0}\alpha\right)B_{\max}, \tag{3}$$

– if $0.8\alpha < \alpha < 0.5\alpha_d$

$$B(\alpha) = B_{\max}, \tag{4}$$

where: $\beta = B_0/B_{\max}$, α is the angle of the stator slot opening in relation to the rotor circumference [4], $\alpha_0 = 2b_s/d = b_s/r_s$, d is the inner stator diameter, r_s is the inner stator radius.

In a salient pole synchronous generator the magnetic rotor asymmetry (in the direct and quadrature axes) and the shape of a pole shoe with various lengths of an air gap and with the bars of the damping cage (placed inside the pole shoes) mean that the air gap is more complex than in cylindrical or asynchronous generators. The air gap length has a significant influence on the magnetic flux density distribution and on the induced stator voltage waveforms [1-13, 17, 18].

Most frequently, the pole shoes in a salient pole synchronous generator are made of solid iron or with electrotechnical sheets (up to 2.5 mm in thickness) [14].

The presence of a rotor damping cage during the cooperation of a synchronous generator with a power grid allows the shortening of many transient processes [19-21] and the presence of a damping cage is not a subject of discussion. But in the case of the synchronous generator set (working as a back-up power system), the presence of a damping cage is debatable particularly in the no-load state. The damping cage can be made of solid iron [14].

Apart from the stator and rotor slotting and the type of stator and rotor windings and damping cage, the inner eccentricity of the stator and rotor has an influence on the distribution of the magnetic flux density in the air gap of a salient pole synchronous generator. This problem is widely discussed in many papers [22-25].

Because of the small initial length of the air gap, the influence of the air gap length on the eddy currents and power loss in the solid elements in low-power synchronous generators is more visible than in high-power ones. The depth of eddy current penetration λ is determined as [14, 15]:

$$\lambda = \frac{5 \cdot 10^5}{\sqrt{f \gamma \mu_r}}, \tag{5}$$

where: f is the frequency, γ is the electrical conductivity, μ_r is the relative magnetic permeability.

Frequently, electrotechnical sheets are used as a method of eddy current reduction in pole shoes [14]. The other method of reducing the eddy currents shown in this paper is by making radial incisions across the width of the pole shoe [18]. According to expression (5), the depth of an incision across the width of the pole shoe depends on the frequency of the magnetic field and the type of rotor material (its electrical conductivity and magnetic permeability).

This paper presents the influence of the pole shoe radial incision across the width of the pole shoe:

– on the distribution of the normal magnetic flux density in the air gap of a 5.5 kVA salient pole synchronous generator,

– on the waveform of voltages induced in the stator windings.

The air gap length δ between the stator and solid pole shoe in relation to the initial length of the air gap in the longitudinal axis of the examined 5.5 kVA salient pole synchronous generator is expressed as [18]:

$$\delta = \frac{\delta_0}{\cos\alpha}, \tag{6}$$

where: δ is the air gap length between the stator and solid pole shoe, δ_0 is the initial length of the air gap in the longitudinal axis, α is the electrical angle of the pole shoe which is calculated in relation to the longitudinal axis.

The visualization of air gap length δ between the stator and solid pole shoe and the depth of incision δ_i across the width of the pole shoe in relation to the initial length of air gap δ_0 and inner stator radius r_s are shown in Fig. 1.

Fig. 2 shows the relative influence of the air gap length δ (6) and of radial incision of a pole shoe on the effective air gap length in relation to inner stator radius r_s and diameter d vs. the electrical angle of the pole shoe α in relation to the longitudinal axis.

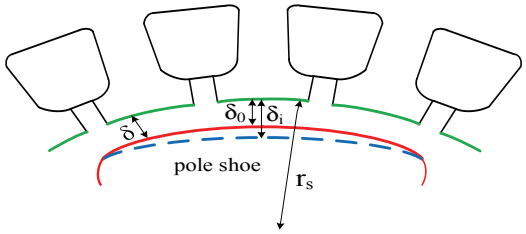

Fig. 1. Visualization of the air gap length δ and the depth of incision δ_i across the width of a pole shoe in relation to the initial length of the air gap δ_0 and inner stator radius r_s

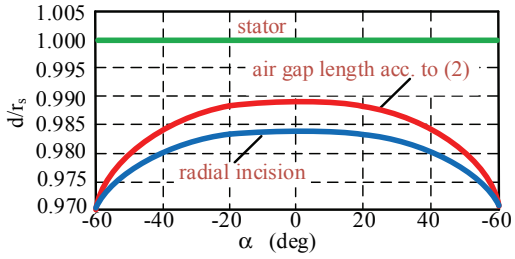

Fig. 2. Relative influence of the air gap length δ and the radial incision δ_i of a pole shoe in relation to inner stator radius r_s and diameter d vs. electrical angle α of the pole shoe

The introduction of the radial incisions on the pole shoe surface results in even loss of the steel (Figs. 1 and 2) and has the effect of flattening the resultant magnetic flux density in the air gap [14, 18]. The effect of flattening the resultant magnetic flux density due to the radial incisions on the pole shoe surface has a similar effect to the case of the pole shoe saturation [14, 18]. The advantage of radial incisions on the solid rotor on the pole shoe surface is that the incisions can be done by utilising a simple lathe. The depth of the radial incisions on the examined rotor circumference is equal to $2\delta_0$ (Fig. 2).

Due to the complex air gap, more detailed results are obtained using Finite Element Method (FEM) software for 2D or 3D models [12, 26]. Simulations of the magnetic flux density distribution and induced voltages with the FEM software are very similar to the results of experimental investigations due to the fact that the FEM models include many construction details [11, 12]. But the FEM calculations also have many disadvantages, for example [11, 12, 27, 28]:

– the length of time required for the calculations in FEM programs is longer than in an analytical way,
– commercial FEM programs are very expensive and require detailed knowledge about the construction of the electrical machine,
– FEM models require a large number of constructional details,
– for a beginner or even a person with intermediate skills, considering which electromagnetic parameters have a direct influence on the final results is difficult.

Therefore, simulations of the magnetic flux density distribution and induced voltages in electrical machines are often carried out by means of both analytical expressions, circuital models and/or FEM software [3, 5-12, 27-29].

In this paper the simulation of the magnetic flux density distribution and experimental investigations of induced voltages are carried out for the salient pole synchronous generator rated: $S_N = 5.5$ kVA, $U_N = 400$ V (Y), $I_N = 7.9$ A, $\cos\varphi_N = 0.8$, $n_N = 3000$ rpm, the number of pole pairs $p_b = 1$, the number of stator slots $Q_s = 24$ with a single-layer winding, rotor: with and without the skew angle $\alpha_q = 15°$ (the skew angle is equal to a single stator tooth pitch). Moreover, magnetic flux density distributions are determined in the air gap of the examined 5.5 kVA salient pole synchronous generator after creating the geometry of the 2D field model in the FEMM program [9, 11-13, 26]. In calculations of the distribution of the magnetic flux density the presence of eddy currents is omitted in the 2D field model due to the powering of the field winding by DC nominal current at no-load $I_{f0N} = \text{const}$.

2. Distributions of magnetic flux density

The distribution of the magnetic flux density lines is obtained taking into account the non-linear material properties. Fig. 3 shows two no-load magnetisation characteristics obtained from the measurement set for the 5.5 kVA salient pole synchronous generator with two rotor structures. One of the no-load characteristics is for a salient pole synchronous generator with a factory rotor made of insulated electrotechnical sheets and the second one is for a generator with a solid rotor with radial incisions.

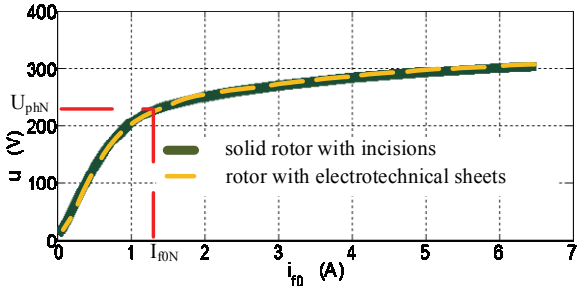

Fig. 3. Comparison of the two no-load magnetisation characteristics of the 5.5 kVA salient pole synchronous generator with two rotor structures obtained from the measurement set

Figure 3 shows that the presented no-load characteristics are very similar.

Figures 4 and 5 show the distribution of the magnetic flux density lines of the examined 5.5 kVA nonlinear salient pole synchronous generator in the no-load steady state in the Finite Element Method Magnetics (FEMM) freeware program [26]. The magnetic flux density lines are obtained from DC current I_{f0N} flowing in the field winding. In the FEMM 2D software, the skew effect in the normal component of magnetic flux density distributions is obtained by subdividing the active rotor length into 79 skewed axial slides along the axial length (39 radial

incisions and 40 without radial incisions – detailed in Fig. 9b). The normal component of magnetic flux density B_{ns} with the rotor skewed slots is calculated as [7]:

$$B_{ns} = \frac{1}{\alpha_q} \int_{\theta-\frac{\alpha_q}{2}}^{\theta+\frac{\alpha_q}{2}} B_n \partial\theta \,, \tag{7}$$

where: α_q is the electrical skew angle, B_{ns}, B_n are the normal component of magnetic flux density in a non-skewed and skewed rotor, respectively.

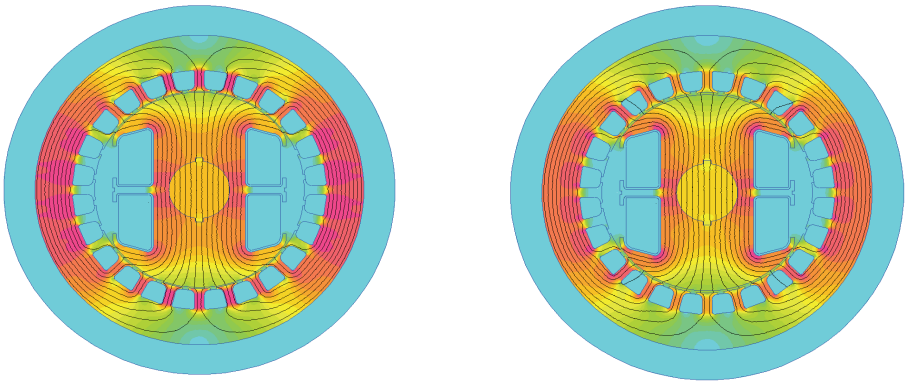

(a) (b)

Fig. 3. General view of the distribution of the magnetic flux density lines in the no-load steady state in the examined 5.5 kVA salient pole synchronous generator: with solid rotor without radial incisions (a), with solid rotor with radial incisions (b)

The distribution of the magnetic flux density lines of the examined 5.5 kVA nonlinear salient pole synchronous generator with the rotor made of 0.5 mm insulated electrotechnical sheets (with an air gap as in the case of the solid rotor without radial incisions) is the same as shown in Fig. 4a.

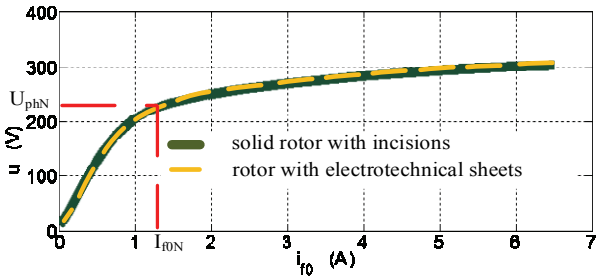

Fig. 4. Comparison of the two no-load magnetisation characteristics of the 5.5 kVA salient pole synchronous generator with two rotor structures obtained in the measurement set

Differences in the distribution of the magnetic flux density are more evident in Fig. 5 (detailed view of the air gaps) and in Fig. 6, where the comparison of the distribution of the normal component of magnetic flux density in the air gap vs. the circumference of the two rotor types is shown.

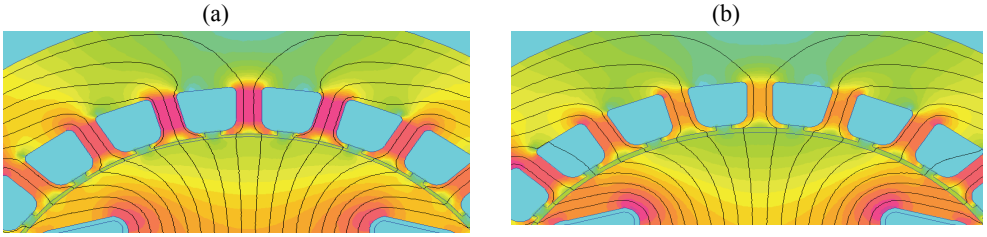

Fig. 5. Detailed view of the distribution of the normal component of magnetic flux density lines in the no-load steady state in the air gap with rotor: without radial incisions (a), with radial incisions (b)

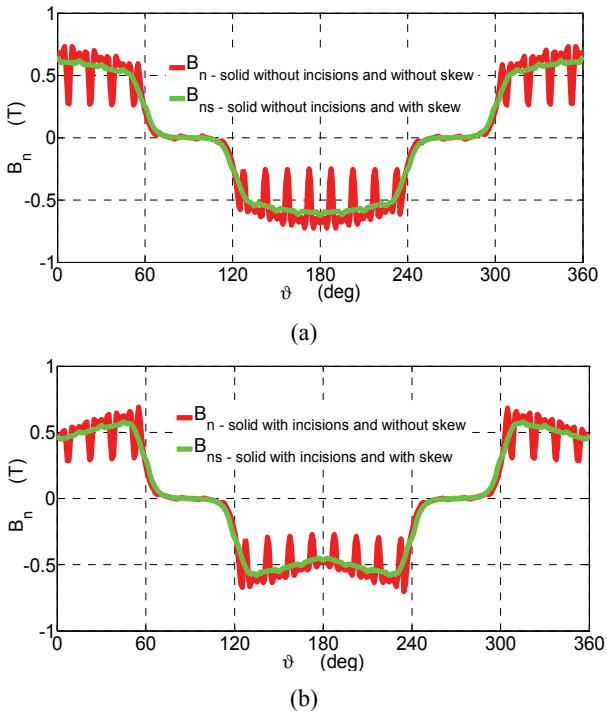

Fig. 6. Comparison of normal component of magnetic flux density distributions for the examined synchronous generator with: a non-skewed and skewed solid rotor (a), a non-skewed and skewed solid rotor with the radial incision (b)

Fig. 6 shows a comparison of the distribution of the normal component of magnetic flux density in the air gap for the synchronous generator with and without the radial incisions and with and without the skew angle. The distribution of the normal component of magnetic flux

density in the air gap for the 5.5 kVA synchronous generator with a rotor made of insulated 0.5 mm electrotechnical sheets gives the same result as in the case of the solid rotor without radial incisions.

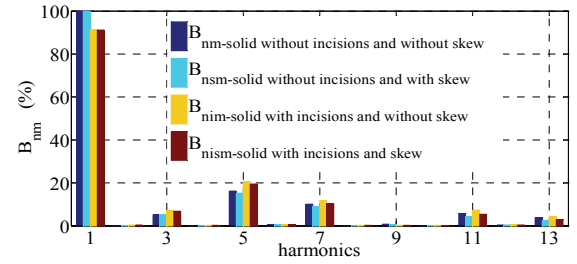

(a)

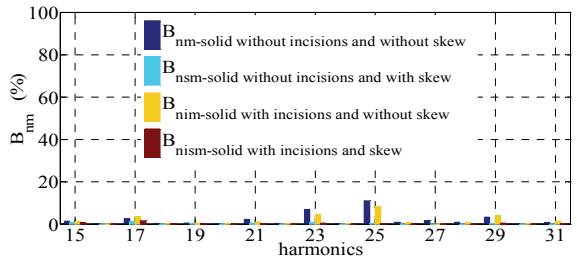

(b)

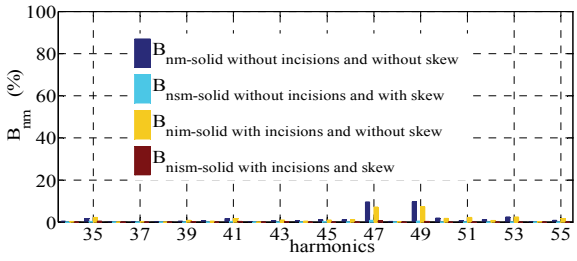

(c)

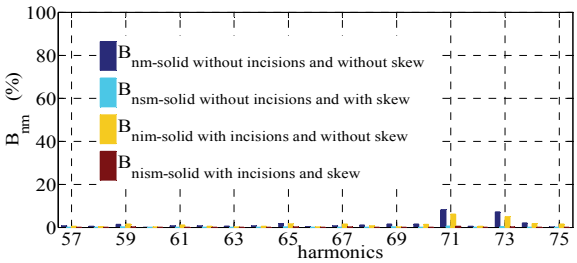

(d)

Fig. 7. Comparison of harmonic contents in the normal component of magnetic flux density distributions: from 1st to 13th order (a), from 15th to 31st order (b), from 35th to 55th order (c), from 57th to 75th order (d)

The distribution results presented in Fig. 6 show that in the areas with a longer air gap the flux density distributions decrease but in the areas with a smaller air gap they increase (Fig. 5b). The variations in the distribution of the normal component of the magnetic flux density shown in Fig. 6 are caused by a permeance change between the stator teeth and slots on the circumference of the stator and rotor (Fig. 5).

Figure 7 shows the comparison of the magnitude of harmonic contents in the magnetic flux density distributions (Fig. 6) due to the Fourier analysis.

The comparisons shown in Fig. 7 are determined in relation to the amplitude of the fundamental component of the magnetic flux density distribution in the air gap for the synchronous generator with a solid rotor without incisions and without skewed poles. The results in Fig. 7 reveal that the $2\delta_0$ radial incision causes:

– 10% reduction of the magnetic flux density fundamental component (Fig. 7a),

– an increase of the odd harmonics up to the 17th order by a few percent,

– a reduction of the $kQ_s \pm 1$ higher harmonic amplitudes by a few percent (k is integer number).

The number of radial incisions has an influence on the increase of the odd harmonics up to the 17th order (Fig. 7). The radial incisions, which are the percentage loss of steel along the length of the pole shoe, changed the v-th harmonics of the magnetic flux density from B_{nv} (for the non-skewed rotor without incisions) to B_{niv} (for the non-skewed rotor with incisions) and from B_{nsv} (for the skewed rotor without incisions) to B_{nisv} (for the skewed rotor with incisions).

The effect of flattening the equivalent air gap between the stator and the pole shoe (with the radial incision) can be reduced by incisions defined according to the relation (6). But such incision must be made with numerically controlled machine tools instead of a typical lathe. The normal component of the magnetic flux density distributions for the examined 5.5 kVA synchronous generator, as presented in Fig. 6, has an impact on the content of higher harmonics in the induced stator phase voltages. As was shown in [9, 18], the wave-shape of the induced stator phase voltages is influenced not only by the magnetic flux density distributions (Fig. 5) but also by the winding coefficient (which for a single-layer winding depends on the winding distribution, slot opening and rotor skew coefficients).

3. Voltages induced in the stator windings

In the no-load state of the salient pole synchronous generator (currents i_a, i_b and i_c are equal to zero) without the power grid and a damping cage, voltages: u_a, u_b, u_c induced in the stator windings and u_f in the field winding, taking into account the electrical angle of the rotor position θ, can be derived for the stator windings (in stator coordinates) and for the field winding in rotor coordinates [11, 12]

$$\frac{\mathrm{d}\Psi_a(\theta, i_f)}{\mathrm{d}t} = u_a\,, \quad \frac{\mathrm{d}\Psi_b(\theta, i_f)}{\mathrm{d}t} = u_b\,, \quad \frac{\mathrm{d}\Psi_c(\theta, i_f)}{\mathrm{d}t} = u_c\,, \tag{8}$$

$$\frac{\mathrm{d}\Psi_f(\theta, i_f)}{\mathrm{d}t} + R_f i_f = u_f\,, \tag{9}$$

$$\frac{\mathrm{d}\theta}{\mathrm{d}t} = \omega\,, \tag{10}$$

where: a, b, c and f are the indexes of stator windings and field winding, u_a, u_b, u_c and u_f are the stator phase voltages and field voltage, Ψ_a, Ψ_b, Ψ_c and Ψ_f are the stator and field linkage fluxes, θ is the electrical angle of the rotor position, $\theta = \theta_m p$, θ_m is the mechanical angle of the rotor position, $\omega = \mathrm{d}\theta/\mathrm{d}t$ is the electrical angular velocity, R_f is the resistance of the field winding, i_f is the field current, p is the number of pole pairs.

Based on expressions (8)-(10) and the relations between the magnetic fluxes and magnetic flux densities and taking into account ω = const and $i_f = I_{f0N}$ = const (I_{f0N} – nominal field current at no-load), the induced phase stator voltages u_a, u_b, u_c and u_f can be expressed as:

$$\left.\begin{aligned} 2N_s k_w \frac{r_s l_s}{p}\frac{\partial B_a(\theta)}{\partial\theta}\frac{\mathrm{d}\theta}{\mathrm{d}t} &= u_a,\\ 2N_s k_w \frac{r_s l_s}{p}\frac{\partial B_b(\theta)}{\partial\theta}\frac{\mathrm{d}\theta}{\mathrm{d}t} &= u_b,\\ 2N_s k_w \frac{r_s l_s}{p}\frac{\partial B_c(\theta)}{\partial\theta}\frac{\mathrm{d}\theta}{\mathrm{d}t} &= u_c, \end{aligned}\right\} \tag{11}$$

$$2N_f k_{wf} \frac{r_r l_r}{p}\frac{\partial B_f(\theta)}{\partial\theta}\frac{\mathrm{d}\theta}{\mathrm{d}t} + R_f i_f = u_f\,, \tag{12}$$

where: B_a, B_b, B_c and B_f are the stator and field density of magnetic fluxes with and without the rotor skew (eg. Fig. 6), N_s, N_f are the number of stator and field windings, r_s, r_r are the inner stator and outer rotor radius, l_s, l_r are the length of stator and rotor, k_w is the winding factor: $k_w = k_d\, k_p\, k_b\, k_q$ [9, 14], k_d is the distribution factor, k_p is the pitch factor, k_{bv} is the slot opening factor, k_{qv} is the skew factor, k_{wf} is the field winding factor.

The problem of the influence of the pitch- and winding distribution, and slot-opening and slot-skewing winding factors (of the 5.5 kVA salient pole synchronous generator) on the reduction of the harmonic contents in induced stator voltages in the most frequently used windings: single-layer, double-layer and triangular, is widely discussed in [9].

Fig. 8 shows the comparison of the lower order harmonics of magnetic flux density (shown in Fig. 6) and magnetic flux density derivatives for the synchronous generator with a solid rotor without incisions. Lower order harmonics of magnetic flux density for the generator with solid rotor with incisions are very similar to ones presented in Fig. 8 and are omitted. The differences in magnitudes of the harmonics are better visible in Fig. 7. Fig. 8 shows that the ν-harmonic presence in magnetic flux density is enhanced ν-times in magnetic flux density derivatives. The ν-harmonic in magnetic flux density enhanced ν-times by derivatives has significant influence on the increase of the harmonic content in the induced stator voltages-expression (11).

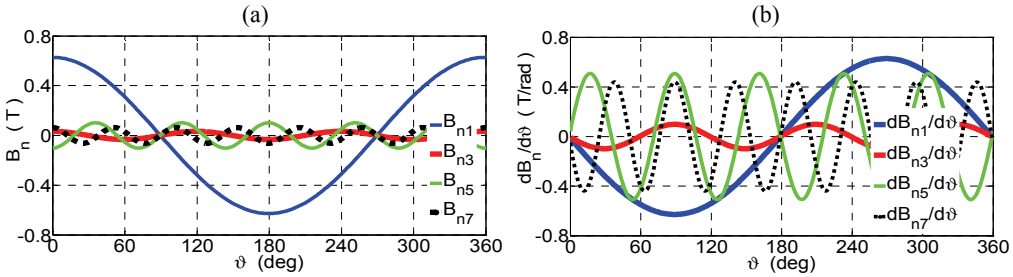

Fig. 8. Comparison of the lower order harmonics: of magnetic flux density (a), magnetic flux density derivatives (b)

Fig. 9 presents winding coefficients for a single layer three-phase winding [9]. The following parameters of the 5.5 kVA synchronous generator are used in calculation of the winding factors of the harmonic v [9]: the number of phases $m = 3$, the number of pole pairs $p_b = 1$, the number of stator slots $Q_s = 24$, the stator slot opening $b_s = 3$ mm, the coil pitch in per unit $y = 1$.

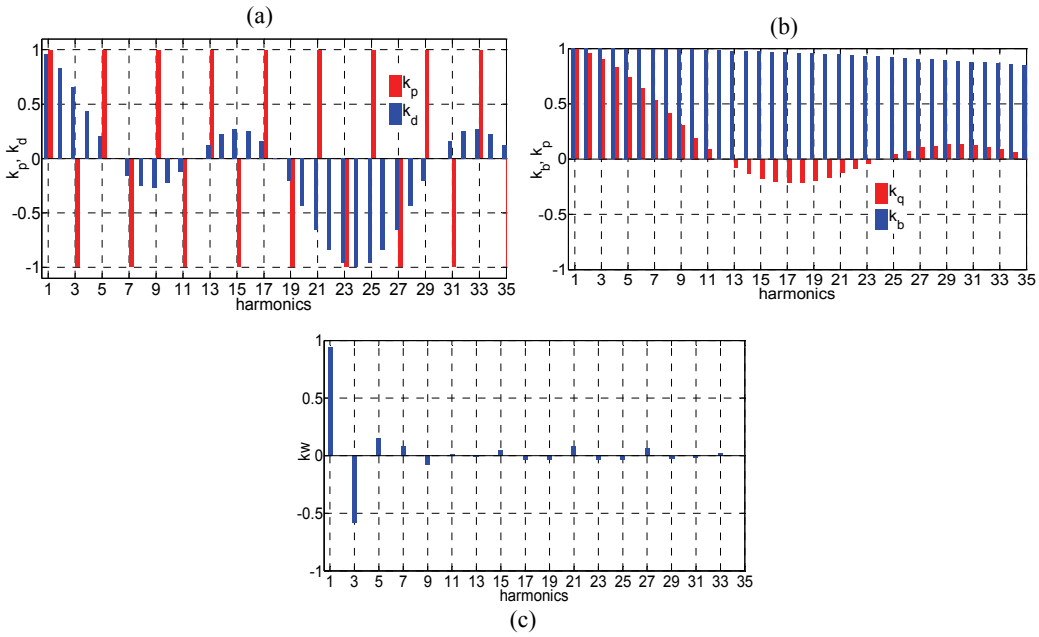

Fig. 9. Winding factors for single layer winding of the 5.5 kVA synchronous generator: k_p and k_d (pitch and distribution factors) (a), k_b and k_q (slot opening and skew factors) (b), $k_w = k_p\,k_d\,k_b\,k_q$ (total factor) (c)

Fig. 10 presents the waveforms of the induced stator voltages of the examined 5.5 kVA salient pole synchronous generator in no-load state calculated in Matlab from expression (11)

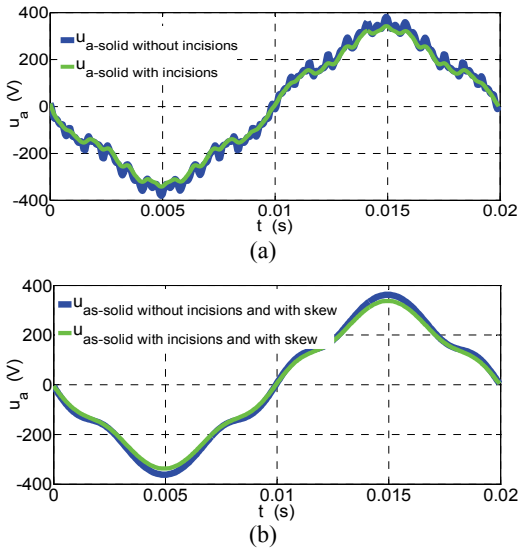

Fig. 10. Waveforms of the induced stator voltages under no-load conditions for the examined 5.5 kVA synchronous generator with the following rotors: solid, skewed and non-skewed (a), solid, skewed and non-skewed with radial incisions (b)

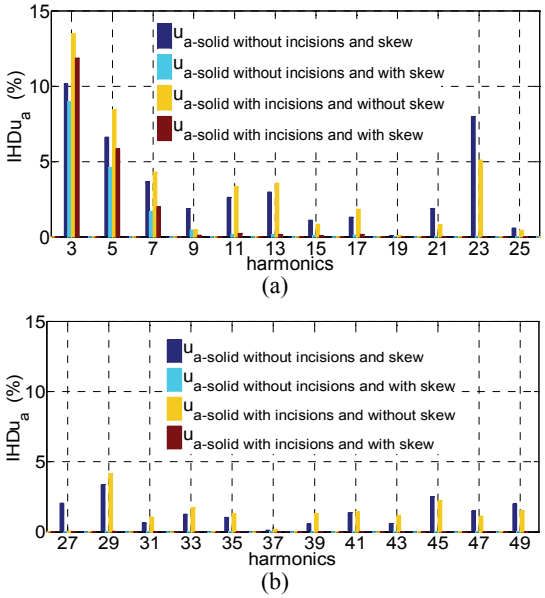

Fig. 11. Individual harmonic distortion of the induced stator voltages under no-load conditions for the examined 5.5 kVA synchronous generator: from 3rd to 25th order (a), from 27th to 49th order (b)

and utilising the normal component of magnetic flux density distributions (presented in Fig. 6 for the synchronous generator with the following rotor structures: solid with and without skew, solid with and without radial incisions). Fig. 10 presents the calculated waveforms of

the induced stator voltages only in phase *a*. Voltages u_b and u_c are very similar to u_a (Fig. 10) and are shifted by the electrical degree of $2\pi/3$. Moreover, Fig. 11 presents the individual harmonic distortion $IHDu_a$ in relation to the fundamental component of the induced stator voltages of the synchronous generator with the non-skewed solid rotor.

Comparing the induced stator voltages (Fig. 10), the magnetic flux density derivatives (Fig. 8) and the winding factors (Fig. 9) it can be concluded that the higher harmonic content is primarily influenced by the product of the electrical angular velocity ω and derivatives of magnetic flux density $\partial B/\partial\theta$. The product $\omega(\partial B/\partial\theta)$ is reduced by the winding factors (Fig. 9). The greatest reduction of the harmonic content in the induced stator voltages is achieved by skewing the rotor (Fig. 10c). The rotor skewness has a very small influence on harmonic reduction of the 3rd and 5th order harmonics (Figs. 9-11).

4. Experimental investigations

Experimental investigation of the influence of the rotor incisions on the waveforms of induced stator voltages of the 5.5 kVA salient pole synchronous generator is carried out by comparison of the induced stator voltages for the three rotor structures shown in Fig. 12. Fig. 12 shows [18]:

– a non-skewed solid rotor,

– a non-skewed solid rotor with 39 radial incisions,

– a skewed rotor with insulated electrotechnical sheets and open (not shorted) damping bars.

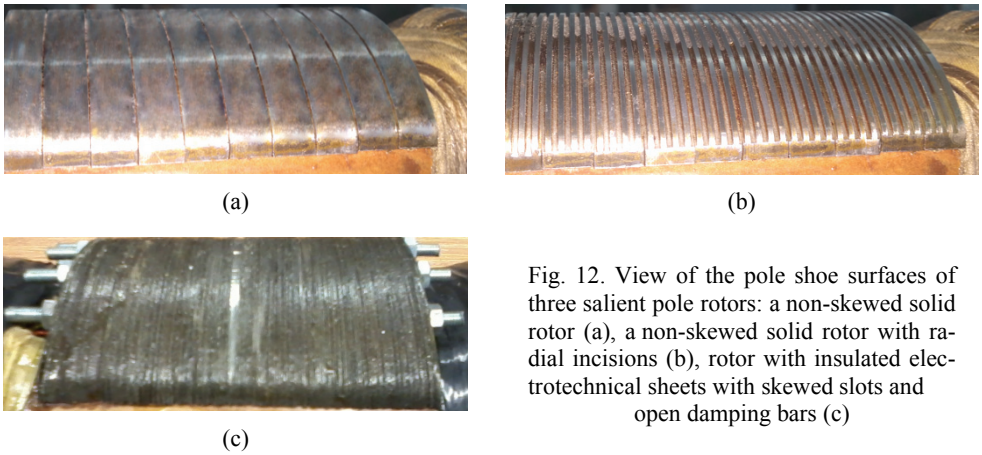

(a) (b) (c)

Fig. 12. View of the pole shoe surfaces of three salient pole rotors: a non-skewed solid rotor (a), a non-skewed solid rotor with radial incisions (b), rotor with insulated electrotechnical sheets with skewed slots and open damping bars (c)

Experimental investigations of the 5.5 kVA salient pole synchronous generator with the three rotor structures are carried out using the measurement set shown in Fig. 13.

Fig. 14 presents a simplified block diagram of the measurement set (shown in Fig. 13).

Fig. 13. General view of the measurement set used for the investigation of the 5.5 kVA salient pole synchronous generator with the three rotor structures

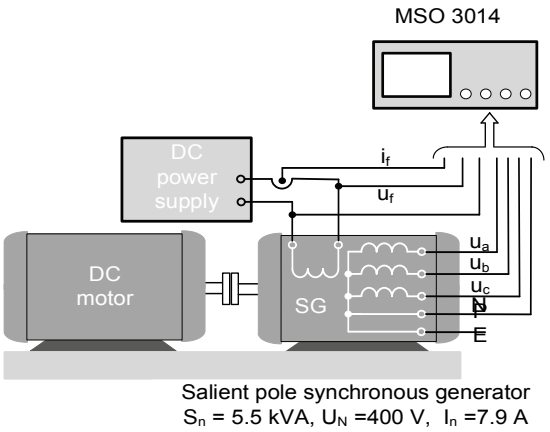

Fig. 14. Simplified block diagram of the measurement set used for the investigation of the 5.5 kVA salient pole synchronous generator

Fig. 15 presents the registered waveforms of the induced stator voltages and the field voltage as well as the current of the examined 5.5 kVA salient pole synchronous generator in no-load state. During the experimental investigations the synchronous generator was running with the following rotor structures: solid, non-skewed, solid, non-skewed with radial incisions, and skewed with insulated electrotechnical sheets. Moreover, the field winding of the examined 5.5 kVA salient pole synchronous generator for all cases was powered by a DC voltage source (U_f = const-shown in Fig. 15c) for the same RMS value of 230 V of the fundamental component phase stator voltages. As shown in [11], when powering the field winding of the 5.5 kVA salient pole synchronous generator, in induced u_a, u_b and u_c voltage waveforms (11) in no-load state, the total harmonic distortion *THDu* is the lowest. So, during the experimental investigations the field winding of the examined 5.5 kVA salient pole synchronous generator is powered using a DC voltage source.

Fig. 16 shows a comparison of the individual harmonic distortion ($IHDu_a$) in the induced stator voltages in phase *a* shown in Fig. 15. $IHDu_a$ is calculated due to the Fourier analysis of voltage u_a with respect to the fundamental component.

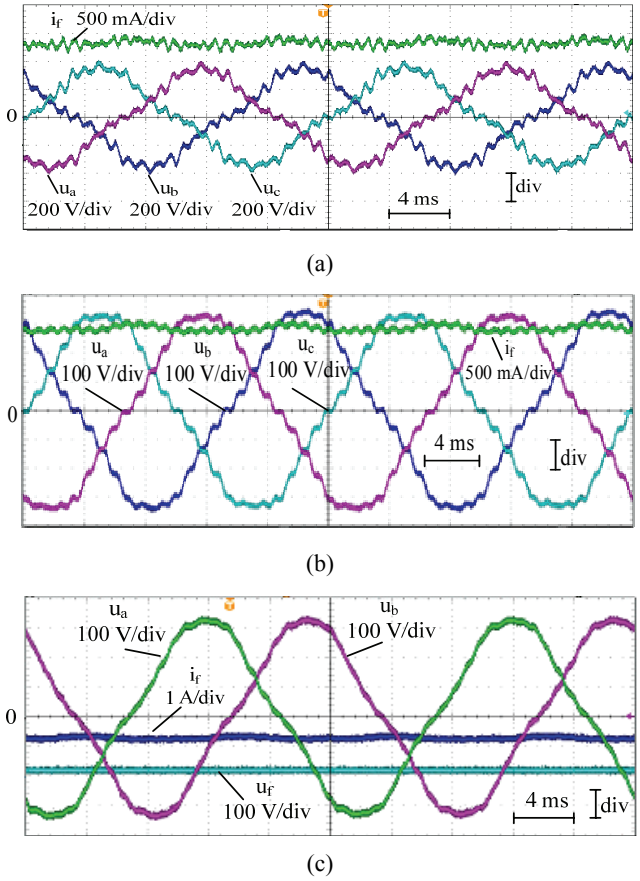

Fig. 15. Waveforms of the induced stator voltages under no-load conditions for the examined 5.5 kVA salient pole synchronous generator with the following rotors: solid, non-skewed (a), solid, non-skewed with radial incisions (b), skewed, made of electrotechnical sheets (c)

Based on the presented waveforms in the induced voltages in the stator winding in no-load state of the examined 5.5 kVA salient pole synchronous generator (Fig. 15) and on individual harmonic distortion (Fig. 16), the total harmonic distortion (THDu_a, THD$u_{a\text{-}ri}$ and THD$u_{a\text{-}e}$) counted up to the 75th harmonic is equal to:

– THDu_a = 16.39% for the generator with a solid, non-skewed rotor without radial incisions (THD$u_{a\text{-}c}$ = 17.23% calculated for generator with the same rotor construction – details Fig. 11),

– THD$u_{a\text{-}ri}$ = 9.58% for the generator with a solid, non-skewed rotor with radial incisions (THD$u_{a\text{-}ri\text{-}c}$ = 18.34% calculated for generator with the same rotor construction – details Fig. 11),

– THD$u_{a\text{-}e\text{-}s}$ = 9.30% for the generator with a skewed rotor made of electrotechnical sheets (THD$u_{a\text{-}s\text{-}c}$ = 10.35% calculated for a generator with the solid, skewed rotor without incisions – details Fig. 11).

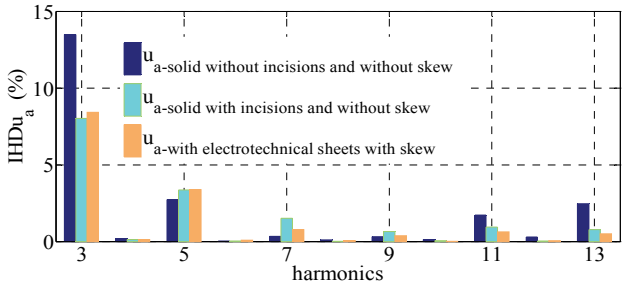

(a)

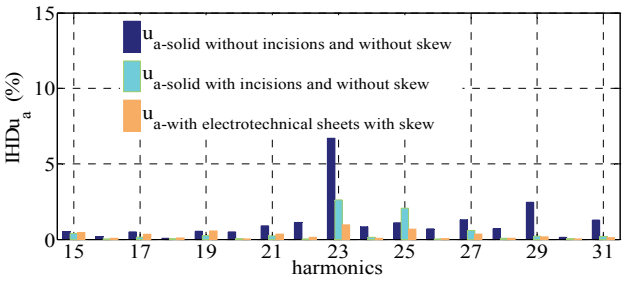

(b)

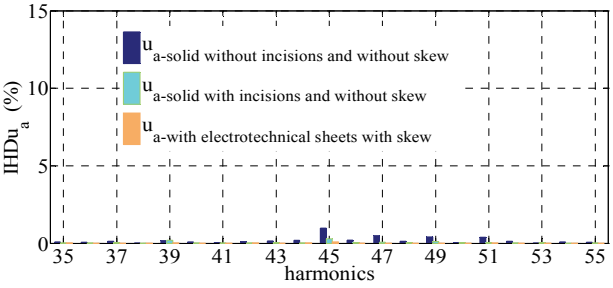

(c)

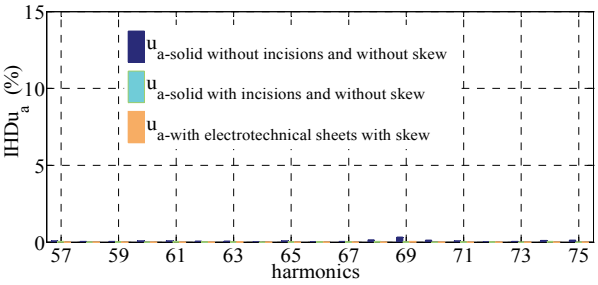

(d)

Fig. 16. Comparison of individual harmonic distortion in the induced voltages in stator winding in no-load state of the 5.5 VA salient pole synchronous generator with three rotor constructions: from 3rd to 13th order (a), from 15th to 31st order (b), from 35th to 55th order (c), from 57th to 75th order (d)

5. Conclusion

The main motivation of this paper is to show the influence of the radial incisions, saliency and the skewness of the rotor and the stator slotting on the higher harmonic contents in the magnetic flux density in the air gap (calculated during simulations in the FEMM program) and in the voltage waveforms induced in the stator winding (registered in a single-layer winding during experimental investigations) in the no-load state of the salient pole synchronous generator. The simulations and experimental investigations were carried out for the low power 5.5 kVA salient pole synchronous generator with a solid, non-skewed rotor, with a solid, non-skewed rotor and radial incisions, and with a skewed rotor made of electrotechnical sheets. Based on the presented comparison of THDu_a and THDu_a for the examined 5.5 kVA synchronous generator, it can be concluded that the introduction of 39 constant depth radial incisions on the rotor solid surface of the pole shoe equal to $2\delta_0$:

– reduces the amplitude of the magnetic flux density by 10% (Figs. 6 and 7),

– increases by 32% the 3rd harmonic in the component of the normal magnetic flux density and reduces by 43% its participation in the induced stator voltages,

– in the induced stator voltages gives a similar higher harmonic spectrum to the case of the generator with the rotor made of electrotechnical sheets.

The higher harmonics that occur in the induced voltages of a single-layer stator winding are v-times lower than in the normal component of the magnetic flux density. This is due to the fact that in the single-layer stator winding the harmonic contents are reduced by pitch, slot opening and skew winding factors.

During the experimental investigation of the three-phase salient pole synchronous generator with a solid, non-skewed rotor with radial incisions, the total harmonic distortion was found to be 9.58%. THD$u_{a\text{-}c}$ obtained from the 2D model in FEMM program (without eddy current) and expression (11) is 18.34%. It means that there are some differences between FEMM's 2D model and the investigated generator that have an influence on the harmonic content. These differences can be explained by:

– different saturation in the 2D model and in the investigated 5.5 kVA synchronous generator,

– omission of eddy currents in rotor poles in the 2D model (eddy currents have a shielding effect on magnetic flux density distribution [30]),

– different shape and nonuniformity of the real air gap along the length of the rotor and stator than in the 2D model.

References

[1] Dajaku G., Gerling D., *Stator slotting effect on the magnetic field distribution of salient pole synchronous permanent-magnet machines*, IEEE Transactions on Magnetics, vol. 46, no. 9, pp. 3676-3683 (2010).

[2] Dajaku G., Gerling D., *Air-gap flux density characteristics of salient pole synchronous permanent-magnet machines*, IEEE Transactions on Magnetics, vol. 48, no. 7, pp. 2196-2204 (2012).

[3] Gaussens B., Saint-Michel J., Lécrivain M., Gabsi M., *Analytical approach for air-gap modeling of field-excited flux-switching machine: No-load operation*, IEEE Transactions on Magnetics, vol. 10, no. 10, pp. 1-13 (2012).
[4] Xiaohua B., Na L., Yong F., Fuying L., *Novel method of evaluation of Carter factor for closed slot submersible motor including fringing effect and magnetic saturation*, Transactions of China Electrotechnical Society, vol. 30, no. 12, pp. 220-227 (2015).
[5] Sobczyk T.J., *Mathematical model of synchronous generators accounting for saturation due to the first and the third MMF harmonic*, 35th International Symposium on Electrical Machines SME'99, 14-16 June, Kazimierz Dolny, Poland, OWPW, Elektryka, no. 111, pp. 43-51 (1999).
[6] Kutt F., Michna M., Ronkowski M., Chrzan P.J., *Non-uniform saturation modelling of synchronous generator pole shoes*, Zeszyty Problemowe Maszyny Elektryczne, no. 103, pp. 121-126 (2014).
[7] Skwarczyński J., Weinreb K., *Method of analysis of slot harmonics in the salient-pole synchronous generators*, International Conference on Electrical Machines (ICEM'1990), Aug. 13-15, Boston MA, USA, pp. 1165-1170 (1990).
[8] Moreira J., Lipo T.A., *Modeling of saturated AC machines including air gap flux harmonic components*, IEEE-IAS Conference Record, 7-12 October, Seattle, Washington, USA, Part 1, pp. 37-44 (1990).
[9] Ludwinek K., *An overview of the most important methods of reducing the harmonic content introduced by discretely distributed armature winding*, Elektro. Info. (in Polish), no. 7-8, pp. 53-57 (2014).
[10] Kutt F., Michna M., Ronkowski M., Chrzan P.J., *Polyharmonic model of synchronous generator for analysis of autonomous power generation systems*, Zeszyty Problemowe Maszyny Elektryczne, no. 92, pp. 109-114 (2011).
[11] Ludwinek K., *Influence of DC voltage and current of field winding on induced stator voltages of a salient pole synchronous generator*, International Review of Electrical Engineering, vol. 9, no. 1, pp. 62-72 (2014).
[12] Ludwinek K., *FEMM utilisation in representation of inductance distributions in a salient pole synchronous generator circuital model in no-load state*, Technical Transactions – Electrical Engineering, vol. 1-E/2015, pp. 325-341 (2015).
[13] Ludwinek K., *Some aspects of inductance distributions modeling in dq0-axes and damping circuits on the rotor of a salient pole synchronous generator*, Technical Transactions – Electrical Engineering, vol. 2-E/2015, pp. 37-52 (2015).
[14] Dąbrowski M., *Design of Alternating Current Electrical Machines*, WNT (in Polish), Warszawa (1994).
[15] Pyrhönen J., Jokinen T., Hrabcová V.P., *Design of Rotating Electrical Machines*, John Wiley & Sons (2014).
[16] Carter F.W., *Note on air gap and interpolar induction*, Journal of Institution of Electrical Engineering, vol. 29, no. 146, pp. 923-933 (1926).
[17] Ludwinek K., *Influence of representation of the stator to rotor mutual inductances on the induced phase voltage waveforms in a salient pole synchronous generator*, Zeszyty Problemowe Maszyny Elektryczne, no. 104, pp. 147-154 (2014).
[18] Ludwinek K., Nadolski R., Staszak J., *Comparison of higher harmonic contents in salient pole synchronous generator with radial incisions on the solid pole surface*, Maszyny Elektryczne – Zeszyty Problemowe, no. 108, pp. 113-119 (2015).
[19] Vicol L., Banyai A., Viorel I.A., Simond J.J., *On the damper cage bars' currents calculation for salient pole large synchronous machines*, 11th International Conference on Optimization of Electrical and Electronic Equipment, May 22-24, Brasov, Romania, pp. 9-14 (2008).
[20] Nadolski R., Staszak J., *Natural hunting pulsations of large power turbogenerators*, Archives of Electrical Engineering, vol. XLV, no. 4, pp. 405-459 (1996).
[21] Bacher J., Maier G., *The shielding effect of the built-in damper cage in a synchronous machine*, International Conference on Renewable Energy and Power Quality (ICREPQ'04), 31 March-02 April, Barcelona, Spain, pp. 250-259 (2004).

[22] Sahoo S.K., Rodriguez P., Sulowicz, M., *Comparative investigation of fault indicators for synchronous machine failures*, International Conference on Electrical Machines (ICEM'2014), September 2-5, Berlin, Germany, pp. 1503-1509 (2014).
[23] Rodriguez P., Sahoo S., Pinto C.T., Sulowicz M., *Field current signature analysis for fault detection in synchronous motors, in diagnostics for electrical machines*, IEEE 10th International Symposium on Electric machines, Power Electronics and Drives (SDEMPED), 1-4 September, Guarda, Portugal, pp. 246-252 (2015).
[24] Raziee S.M., Kelk H.M., Alikhani H.R.R., Omati A., *Air-gap eccentricity effects on harmonic contents of field current in synchronous generators*, International Review of Electrical Engineering, vol. 5, no. 1, pp. 83-89 (2010).
[25] Akbari H., *An improved analytical model for salient pole synchronous machines under general eccentricity fault, Progress in Electromagnetic Research*, no. 49, pp. 389-409 (2013).
[26] http://www.femm.info/wiki/HomePage, accessed November 2015.
[27] Jedryczka C., Szelag W., Demenko A., Wojciechowski R. M., *Description of multiply connected regions with induced currents using T-T method*, Progress in Electromagnetic Research B, no. 43, pp. 279-294 (2012).
[28] Bastos J.P.A., Sadowski N., *Electromagnetic Modeling by Finite Element Methods*, Marcel Dekker, New York (2003).
[29] Gomez E., Roger-Folch J., Gabaldon A., Molina A., *Coupling 2D finite element models and circuit equations using a bottom-up methodology*, ACES Journal, vol. 17, no. 3, pp. 225-231 (2002).
[30] Chung Y., Galyda J., *Effect of Eddy Current in the Laminations on the Magnet Field,* LS Note No. 200, April (1992).